Chin. Phys. Lett. **39**, 076801 (2022)

Infrared Nano-Imaging of Electronic Phase across the Metal–Insulator Transition of $NdNiO_3$ Films

Fanwei Liu(刘凡微)[1†], Sisi Huang(黄思思)[2†], Sidan Chen(陈思丹)[1], Xinzhong Chen(陈欣中)[3], Mengkun Liu(刘梦昆)[3], Kuijuan Jin(金奎娟)[2*], and Xi Chen(陈曦)[1*]

[1]*State Key Laboratory of Low-Dimensional Quantum Physics and Department of Physics, Tsinghua University, Beijing 100084, China*
[2]*Institute of Physics, Chinese Academy of Sciences, Beijing 100190, China*
[3]*Department of Physics and Astronomy, Stony Brook University, Stony Brook, NY 11794, USA*

(Received 14 April 2022; accepted manuscript online 1 June 2022)

$NdNiO_3$ is a typical correlated material with temperature-driven metal–insulator transition. Resolving the local electronic phase is crucial in understanding the driving mechanism behind the phase transition. Here we present a nano-infrared study of the metal–insulator transition in $NdNiO_3$ films by a cryogenic scanning near-field optical microscope. The $NdNiO_3$ films undergo a continuous transition without phase coexistence. The nano-infrared signal shows significant temperature dependence and a hysteresis loop. Stripe-like modulation of the optical conductivity is formed in the films and can be attributed to the epitaxial strain. These results provide valuable evidence to understand the coupled electronic and structural transformations in $NdNiO_3$ films at the nano-scale.

DOI: 10.1088/0256-307X/39/7/076801

Perovskite rare-earth nickelates (RNiO$_3$) are correlated electron systems with charge-transfer type metal–insulator transition (MIT) driven by temperature.[1−3] The mechanism of MIT in RNiO$_3$ involves electronic, magnetic and lattice degrees of freedom[4−6] and is still under debate. The detailed behavior depends on the species of the rare-earth R ion. With decreasing temperature, the transition from a paramagnetic metal to an insulator occurs at $T_{\rm MIT}$.[7−10] A charge order also appears in the insulating phase. At the Néel temperature $T_{\rm N} \leq T_{\rm MIT}$, the spin structure becomes antiferromagnetic.

As a well-studied member of the RNiO$_3$ family, $NdNiO_3$ [Fig. 1(a)] undergoes the metal-to-insulator and paramagnetic-to-antiferromagnetic transitions simultaneously,[11,12] i.e., $T_{\rm N} = T_{\rm MIT}$. The metal–insulator transition is also accompanied by a structural change from orthorhombic ($Pbnm$) to monoclinic ($P2_1/n$) symmetry.[12,13] During the structure transition, the NiO_6 octahedra distorts and rotates. Compared with bulk $NdNiO_3$, epitaxial strain and finite film thickness result in more complications during phase transition in films.[14−16] So far, most data about $NdNiO_3$ films was acquired by macroscopic measurements. Nevertheless more and more evidence indicates that the material exhibits strong spatial inhomogeneity at the nano-scale and microscopy is essential to elucidate the MIT mechanism. For example, recent works[17−19] demonstrate the nanoscale phase coexistence when the $NdNiO_3$ films go through the first-order metal–insulator phase transitions. The phase transition is broadened by disorder such as strain field and therefore occurs over a finite range of temperatures where the fraction of low-temperature phase grows from zero to one as the temperature is lowered. Here we report another scenario that features a continuous transition without phase coexistence when $NdNiO_3$ films go through the metal–insulator transition. The nano-infrared (nano-IR) study is performed on a scattering-type scanning near-field optical microscope (s-SNOM). Such infrared near-field microscopy probes local optical conductivity with nanometer resolution[20,21] and has been successfully applied to the investigation of correlated oxides.[22−24]

The $NdNiO_3$ films were deposited on the (100)-oriented cubic $(La_{0.3}Sr_{0.7})(Al_{0.65}Ta_{0.35})O_3$ (LSAT, $a = 0.3868$ nm) substrates by pulsed laser deposition (PLD). The pseudo-cubic perovskite lattice parameter of bulk $NdNiO_3$ is estimated to be 0.3807 nm.[2] The in-plane lattice mismatch is +1.6%. Compared with $NdNiO_3$ films grown on (110)-oriented $NdGaO_3$ substrates, the $NdNiO_3$ films on the LSAT substrates are under a larger tensile strain.[16] During the film

†These authors contributed equally to this work.
*Corresponding authors. Email: kjjin@iphy.ac.cn; xc@mail.tsinghua.edu.cn
© 2022 Chinese Physical Society and IOP Publishing Ltd

deposition, the LSAT substrate was kept at 650 ℃ under an oxygen atmosphere of 20 Pa. Then the sample was annealed at room temperature under an oxygen pressure of ∼0.01 Pa. The film surface is reasonably flat [see the topography image in Fig. 1(b)] and the RMS roughness is less than 0.5 nm. Figure 1(c) shows the resistance versus temperature (R–T) curve of the 15-nm-thick $NdNiO_3$ film measured by the conventional four-probe method. The first-order transition between orthorhombic and monoclinic symmetry is smeared likely because of the strain field from the substrate. The warming and cooling cycles form a hysteresis loop. The transition occurs over a finite range of temperature from 130 K to 200 K. The resistance at low temperature exponentially depends on temperature, indicating that the film is in the insulating phase. The R–T curve suggests that the first-order metal–insulator transition has been broadened by disorder[25] and the thermal cycles should undergo various meta-stable states along the hysteresis loop. However, the transport measurement does not cover the issue of phase coexistence during the transition, which will be addressed by s-SNOM in this study.

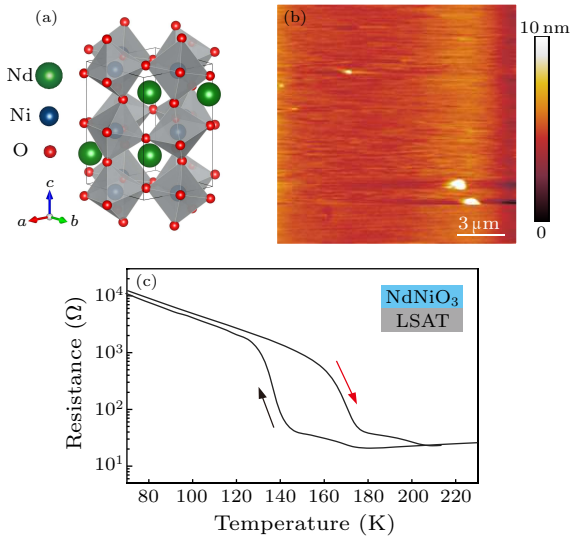

Fig. 1. (a) Crystal structure of bulk $NdNiO_3$. (b) AFM topography[26] of $NdNiO_3$ film with 15 nm thickness at 85 K. (c) Resistance versus temperature from the transport measurement in 15 nm $NdNiO_3$ film. Arrows indicate the direction of transitions on warming (red) and cooling (black).

We employ a cryogenic s-SNOM to investigate the evolution of local electronic properties of $NdNiO_3$ films with temperature. The s-SNOM simultaneously maps the surface morphology and local optical response at the 20 nm scale. The CO_2 laser (p-polarized, $\lambda = 10.26\,\mu$m) is focused on the atomic force microscope (AFM) tip. The mid-IR excitation at 10.26 μm probes dominantly the free-carrier Drude response of $NdNiO_3$ in accordance with far-field spectroscopy.[27,28] The AFM tip is tapping at frequency Ω with an amplitude of ∼50 nm. The local optical response is contained in the scattered signal. The higher harmonics of Ω in the signal, i.e., S_n ($n = 2, 3, \ldots$), are demodulated by a lock-in amplifier (Zurich Instruments, HF2LI) to suppress the far-field background. The self-homodyne detection is used in the nano-IR imaging. Considering its nearly perfect reflectivity in the infrared frequencies,[29] 100 nm gold film is deposited at the sample edge as the reference material to quantify the local optical response.

Figure 2(a) presents the thermal cycle of the infrared nano-imaging for the same region. The spatial average $\bar{S}$ of the near-field signal normalized by gold [$S = S_2(NdNiO_3)/S_2(Au)$] shows significant temperature dependence and a hysteresis loop [Fig. 2(b)]. At the ends of the loop, $\bar{S} = 0.15$ and 0.34, respectively, corresponding to the insulating and conducting phases. The near-field signal is almost homogeneous when the phase transition is completed. During the transition, the inhomogeneity of S is illustrated by the histogram in Fig. 2(c). For each temperature, the counts of pixel as a function of S shows a single peak centered at $\bar{S}$. The peak width is maximized at 150 K and approaches to zero at the end points of the hysteresis in Fig. 1(c). No double-peak structure signifying phase coexistence is observed in the histogram. The inhomogeneity in nano-IR signal distribution only manifests the local fluctuation of conductivity.

The local conductivity fluctuation is more pronounced in the relative nano-IR signal derived from Fig. 2(a). For each temperature of the warming cycle, the image of ΔS ($\Delta S = S - \bar{S}$) is shown in Fig. 3(a) (more data in Fig. S1 and S2 of the Supplementary Material). The full range of the color scale is set to ±15% of $\bar{S}$. The images of S_3 are also shown in Fig. S3 of the Supplementary Material. S_2 is similar to S_3 in the relative signal but with larger absolute magnitude. The stripe-like inhomogeneity along the (011) direction begins to emerge at the onset of phase transition on the R–T curve and eventually disappears at the other end point of the hysteresis. The characteristic width of the stripes is about 2 μm. We propose that the stripe-like modulation is most likely given rise by the balance between the strain energy due to inhomogeneity in the structure during the process of phase transition and that exerted by the substrate. The substrate tends to hinder the phase transition. The competition favors a less uniform distribution of structural transition and slows down the distortion and rotation of octahedra. The frustrated structural change gradually opens or closes the energy gap in the electronic band, leading to a second-order-like metal–insulator phase transition. During the thermal cy-

cle, the stripe-like modulation remains the same but the intensity evolves with temperature [see Fig. 3(b)]. We suggest that the evolution of intensity experiences various meta-stable states pinned by disorder in the process of structural transition, which is responsible for the hysteresis. More theoretical investigation is needed to confirm the above model.

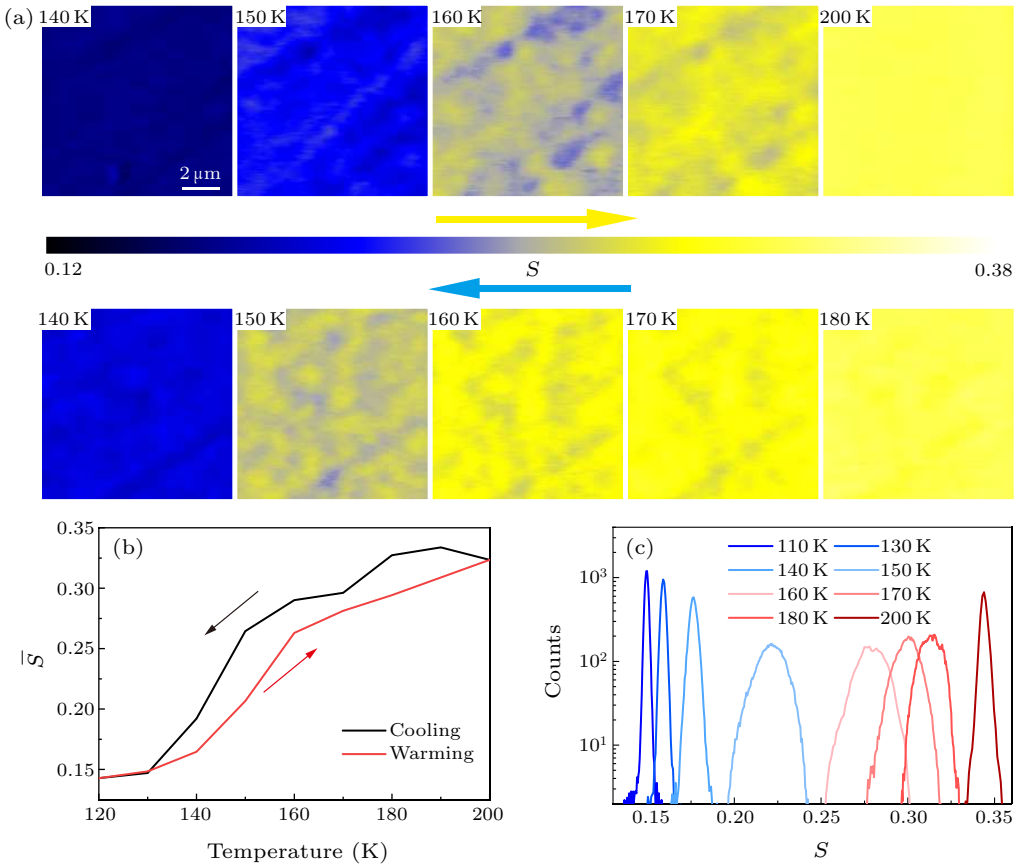

Fig. 2. (a) Images of the normalized nano-IR signal (S) acquired from $NdNiO_3$ film with 15 nm thickness during the warming (top) and cooling (bottom) transition. (b) The spatial average $\bar{S}$ of nano-IR signal through the MIT. Arrows indicate the warming (red) and cooling (black) transition. (c) Histogram representation of the normalized nano-IR signal (S) on warming from 110 K to 200 K.

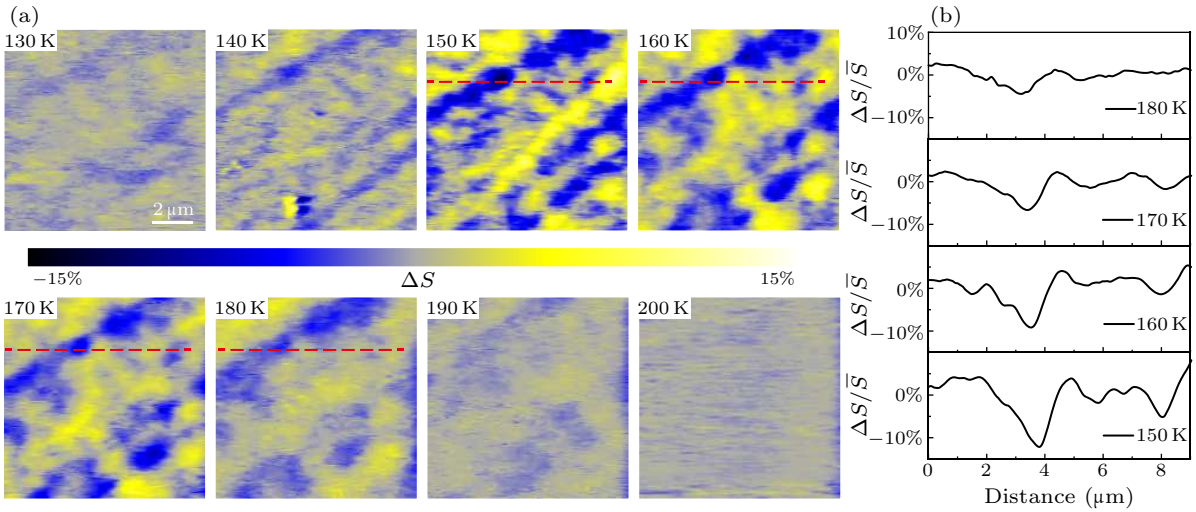

Fig. 3. (a) Images of relative nano-IR signal ($\Delta S = S - \bar{S}$) during the warming transition from $NdNiO_3$ film with 15 nm thickness. All images were acquired in the same field of view. (b) Line profiles (red dashed lines in (a) from 150 K to 180 K) showing the intensity of relative nano-IR signal (ΔS is normalized by $\bar{S}$).

To demonstrate that the above observation generally presents in the $NdNiO_3$ thin films, we perform the experiments with different film thicknesses. Figure 4(a) shows the R–T curve for a 7 nm $NdNiO_3$ film on LSAT prepared under the same growth condition as that of the 15 nm film. The two kinks around 160 K on the R–T curve may be related to an additional phase transition and are still not well understood. The infrared nano-imaging [Fig. 4(b)] and the relative intensity map (Fig. 4(c) and Fig. S4) of the 7 nm film show similar modulation as those of the 15 nm film. The spatial average $\bar{S}$ of the near-field signal normalized by gold ($S = S_2(NdNiO_3)/S_2(Au)$) exhibits a hysteresis loop [Fig. 4(d)]. The temperatures for the end points of the near-field signal loop are close to those of the R–T loop. The loop from 155 K to 190 K is wider than that from 130 K to 155 K possibly as a result of the kinks at 160 K. Once again no indication of phase coexistence is revealed in the histogram for various temperatures [Fig. 4(e)].

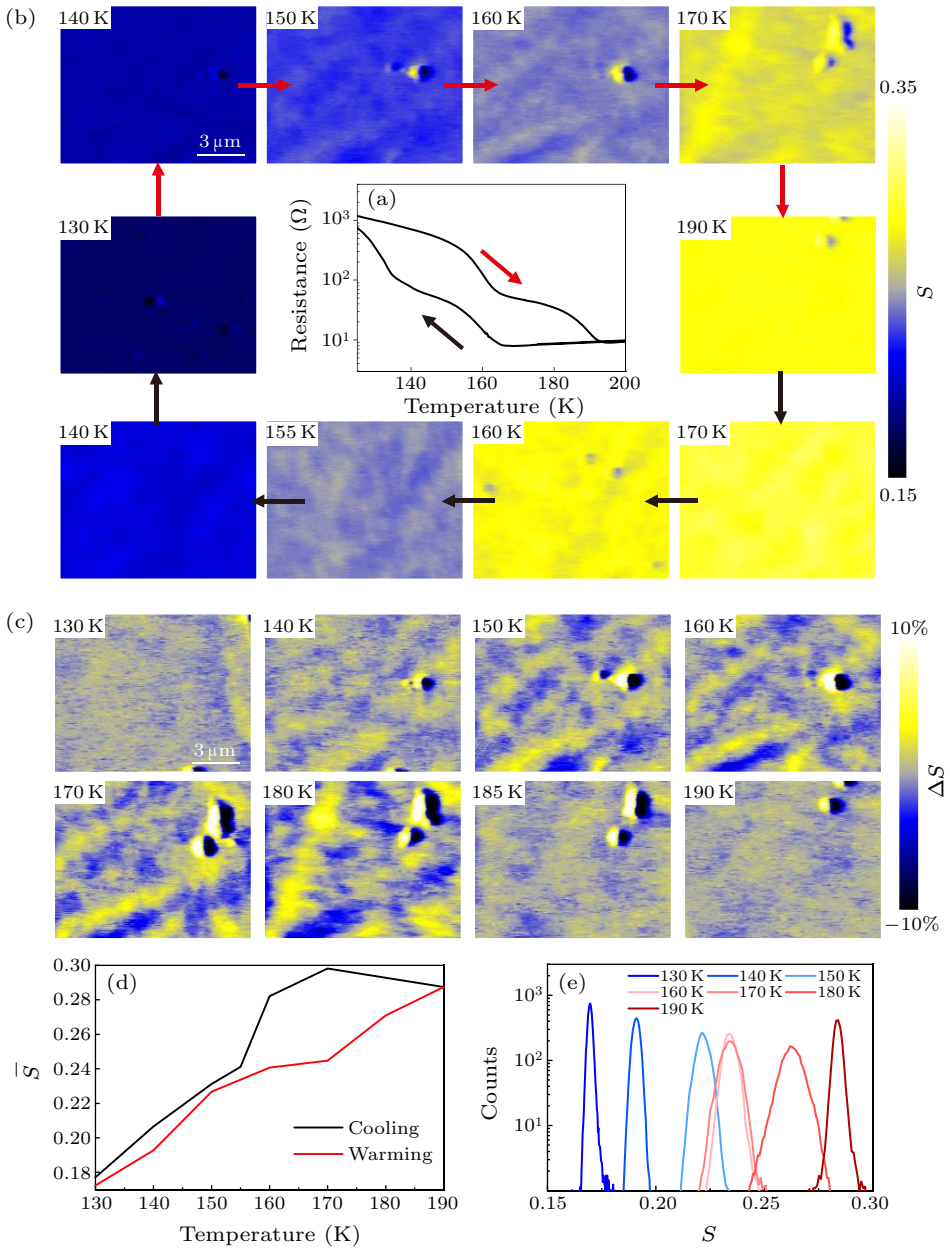

Fig. 4. (a) Temperature dependence of resistance acquired from $NdNiO_3$ films with 7 nm thickness. Arrows indicate the warming (red) and cooling (black) transition. (b) Images of normalized nano-IR signal (S) on warming (red arrows) and cooling (black arrows). (c) Images of relative nano-IR signal (ΔS) on warming. (d) The spatial average $\bar{S}$ of nano-IR signal through the MIT. (e) Histogram representation of the normalized nano-IR signal (S) during the warming transition.

In summary, we have demonstrated the phase transition in the correlated material $NdNiO_3$ at cryogenic temperature by s-SNOM. The $NdNiO_3$ films on the LSAT substrate undergo a continuous transition without phase coexistence across the MIT. Such observation is different from the previous studies and could be due to the different substrates. The emerging stripe-like modulation of optical conductivity during the phase transition is attributed to the hindered structural change. Our study provides new insights into the interplay between electronic and structural degrees of freedom in $NdNiO_3$ films.

References

[1] Torrance J B, Lacorre P, Nazzal A I, Ansaldo E J and Niedermayer C 1992 *Phys. Rev. B* **45** 8209
[2] Medarde M L 1997 *J. Phys.: Condens. Matter* **9** 1679
[3] Catalan G 2008 *Phase Transit.* **81** 729
[4] Alonso J A, García-Muñoz J L, Fernández-Díaz M T, Aranda M A G, Martínez-Lope M J and Casais M T 1999 *Phys. Rev. Lett.* **82** 3871
[5] Johnston S, Mukherjee A, Elfimov I, Berciu M and Sawatzky G A 2014 *Phys. Rev. Lett.* **112** 106404
[6] Bisogni V, Catalano S, Green R J, Gibert M, Scherwitzl R, Huang Y, Strocov V N, Zubko P, Balandeh S, Triscone J M, Sawatzky G and Schmitt T 2016 *Nat. Commun.* **7** 13017
[7] Lee S, Chen R and Balents L 2011 *Phys. Rev. Lett.* **106** 016405
[8] Middey S, Chakhalian J, Mahadevan P, Freeland J W, Millis A J and Sarma D D 2016 *Annu. Rev. Mater. Res.* **46** 305
[9] Ruppen J, Teyssier J, Ardizzone I, Peil O E, Catalano S, Gibert M, Triscone J M, Georges A and Van Der Marel D 2017 *Phys. Rev. B* **96** 045120
[10] Mercy A, Bieder J, Íñiguez J and Ghosez P 2017 *Nat. Commun.* **8** 1677
[11] Caviglia A D, Först M, Scherwitzl R, Khanna V, Bromberger H, Mankowsky R, Singla R, Chuang Y D, Lee W S, Krupin O, Schlotter W F, Turner J J, Dakovski G L, Minitti M P, Robinson J, Scagnoli V, Wilkins S B, Cavill S A, Gibert M, Gariglio S, Z, Triscone J M, Hill J P, Dhesi S S and Cavalleri A 2013 *Phys. Rev. B* **88** 220401
[12] Gawryluk D J, Klein Y M, Shang T, Sheptyakov D, Keller L, Casati N, Ph L, Fernández-Díaz M T, Rodríguez-Carvajal J and Medarde M 2019 *Phys. Rev. B* **100** 205137
[13] Zhang J Y, Kim H, Mikheev E, Hauser A J and Stemmer S 2016 *Sci. Rep.* **6** 23652
[14] Catalan G, Bowman R M and Gregg J M 2000 *Phys. Rev. B* **62** 7892
[15] Xiang P H, Zhong N, Duan C G, Tang X D, Hu Z G, Yang P X, Zhu Z Q and Chu J H 2013 *J. Appl. Phys.* **114** 243713
[16] Liu J, Kargarian M, Kareev M, Gray B, Ryan P J, Cruz A, Nadeem T, Chuang Y D, Guo J H, Rondinelli J M, Freeland J W, Fiete G A and Chakhalian J 2013 *Nat. Commun.* **4** 2714
[17] Mattoni G, Zubko P, Maccherozzi F, van der Torren A J, Boltje D B, Hadjimichael M, Manca N, Catalano S, Gibert M, Liu Y, Aarts J, Triscone J M, Dhesi S S and Caviglia A D 2016 *Nat. Commun.* **7** 13141
[18] Preziosi D, Lopez-Mir L, Li X, Cornelissen T, Lee J H, Trier F, Bouzehouane K, Valencia S, Gloter A, Barthélémy A and Bibes M 2018 *Nano Lett.* **18** 2226
[19] Post K W, McLeod A S, Hepting M, Bluschke M, Wang Y, Cristiani G, Logvenov G, Charnukha A, Ni G X, Padma R, Minola M, Pasupathy A, Boris A V, Benckiser E, Dahmen K A, Carlson E W, Keimer B and Basov D N 2018 *Nat. Phys.* **14** 1056
[20] Qazilbash M M, Brehm M, Chae B G, Ho P C, Andreev G O, Kim B J, Yun S J, Balatsky A V, Maple M B, Keilmann F, Hyun-Tak K and Basov D N 2007 *Science* **318** 1750
[21] Atkin J M, Berweger S, Jones A C and Raschke M B 2012 *Adv. Phys.* **61** 745
[22] Liu M K, Wagner M, Abreu E, Kittiwatanakul S, McLeod A, Fei Z, Goldflam M, Dai S, Fogler M M, Lu J, Wolf S A, Averitt R D and Basov D N 2013 *Phys. Rev. Lett.* **111** 096602
[23] McLeod A S, Van Heumen E, Ramirez J G, Wang S, Saerbeck T, Guenon S, Goldflam M, Anderegg L, Kelly P, Mueller A, Liu M K, Schuller I K and Basov D N 2017 *Nat. Phys.* **13** 80
[24] Mcleod A S, Zhang J, Gu M Q, Jin F, Zhang G, Post K W, Zhao X G, Millis A J, Wu W B, Rondinelli J M, Averitt R D and Basov D N 2020 *Nat. Mater.* **19** 397
[25] Kumar D, Rajeev K P, Kushwaha A K and Budhani R C 2010 *J. Appl. Phys.* **108** 063503
[26] Nečas D and Klapetek P 2012 *Central Eur. J. Phys.* **10** 181
[27] Katsufuji T, Okimoto Y, Arima T, Tokura Y and Torrance J B 1995 *Phys. Rev. B* **51** 4830
[28] Stewart M K, Liu J, Kareev M, Chakhalian J and Basov D N 2011 *Phys. Rev. Lett.* **107** 176401
[29] McLeod A S, Kelly P, Goldflam M D, Gainsforth Z, Westphal A J, Dominguez G, Thiemens M H, Fogler M M and Basov D N 2014 *Phys. Rev. B* **90** 085136

Supplementary Material: Infrared Nano-Imaging of Electronic Phase across the Metal-Insulator Transition of $NdNiO_3$ Films

Fanwei Liu(刘凡微)[1†], Sisi Huang(黄思思)[2†], Sidan Chen(陈思丹)[1], Xinzhong Chen(陈欣中)[3], Mengkun Liu(刘梦昆)[3], Kuijuan Jin(金奎娟)[2*] and Xi Chen(陈曦)[1*]

[1]*State Key Laboratory of Low Dimensional Quantum Physics and Department of Physics, Tsinghua University, Beijing 100084, China*

[2]*Institute of Physics, Chinese Academy of Sciences, Beijing 100190, China*

[3]*Department of Physics and Astronomy, Stony Brook University, Stony Brook, NY 11794, USA*

Cryogenic near-field optical microscope

The homemade AFM assembly (including the parabolic mirror focusing the incident laser light) is mounted on the cooling stage of cryostat (CryoVac). The base temperature of the AFM assembly is 85 K with a liquid nitrogen bath. All measurements were conducted in an ultra-high vacuum ($< 10^{-9}$ mbar) environment to prevent the surface contamination (such as accumulation of dirt and impurity). We use a fiber-coupled interferometer (attocube, LDM1300) to monitor the oscillation of tip. The probes we use are commercially available from Nanoworld (Arrow^{TM} NCPt). The drift of tip oscillation amplitude is about 5% in an hour at 85 K. A DC bias could be applied on the Z-axis piezo-stacks of the tip step motor to continuously adjust the tip position in the range of 100 nm. When the tip position is out of the adjustment range of the DC bias, the step motors are used to recover the amplitude. The challenges for imaging include changes in piezoelectric response of the sample scanner and thermal drift of the sample stage relative to the tip at variable temperatures. We use the standard testing sample TGQ1 (NT-MDT) for the calibration of the imaging distortion at variable temperatures. The position of the sample can be manually adjusted at different temperature. A raw scanning range is often larger than the area of the subsequent statistical measure. By tracking the pixels of the impurities, we can tailor and correct the raw images to acquire signal from the same area at different temperatures.

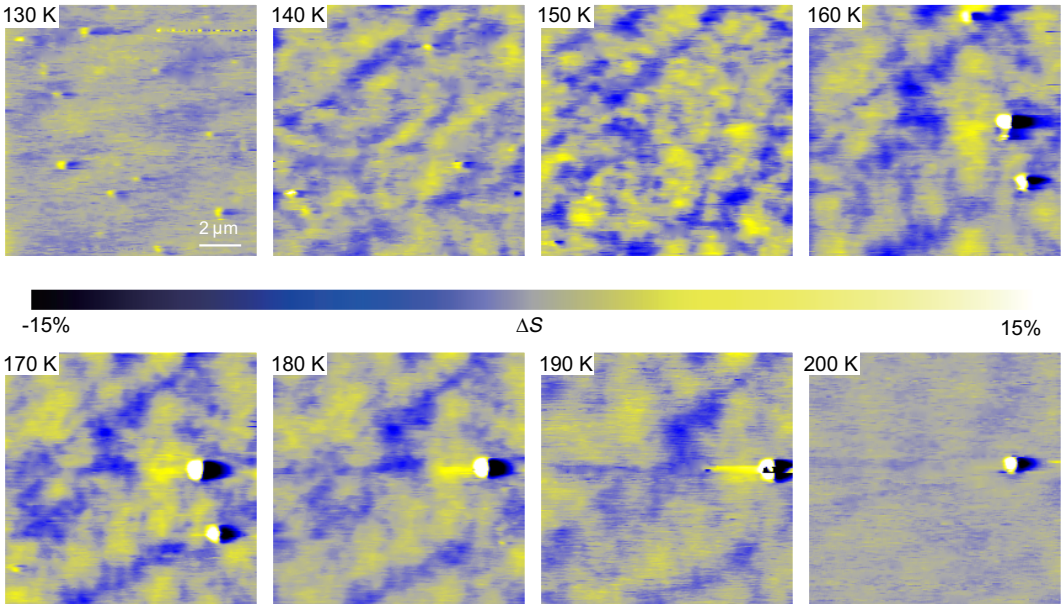

Fig. S1. More images of relative nano-IR signal (ΔS) on warming of $NdNiO_3$ films with 15 nm thickness.

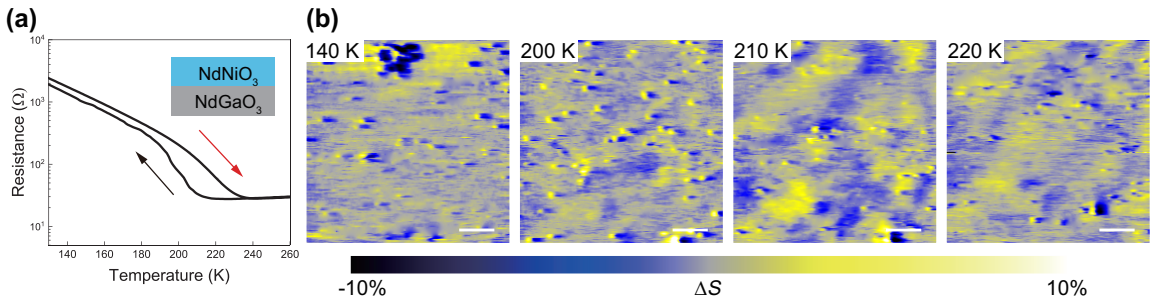

Fig. S2. $NdNiO_3$ films with 15 nm thickness on (100)-oriented $NdGaO_3$ substrate. The in-plane lattice mismatch is +1.8%. (a) Resistance versus temperature from the transport measurement. Arrows indicate the direction of transitions on warming (red) and cooling (black). (b) Images of relative nano-IR signal (ΔS) on warming in the $NdNiO_3$ films with 15 nm thickness. The stripe-like modulation is formed during the phase transition near 210 K.

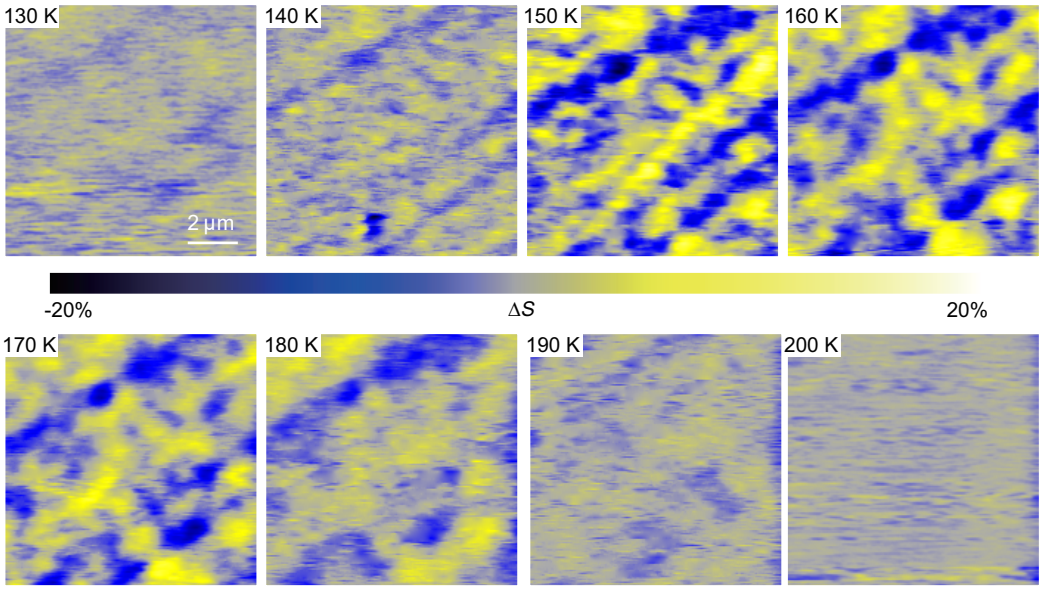

Fig. S3. Images of relative third harmonic nano-IR signal during the warming transition in $NdNiO_3$ films with 15 nm thickness. As a comparision with relative second harmonic nano-IR signal in the same field of view shown in Fig. 3(a).

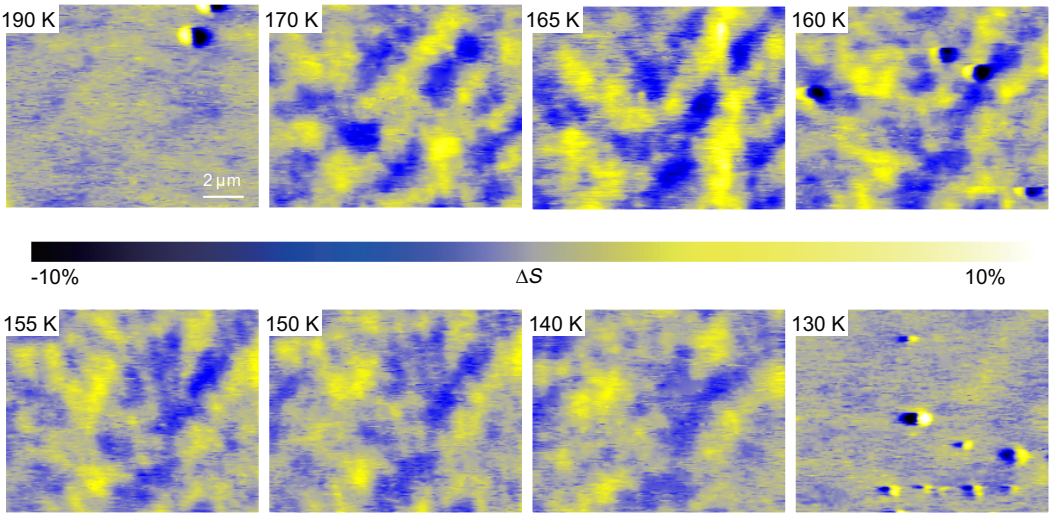

Fig. S4. Images of relative nano-IR signal (ΔS) on cooling in $NdNiO_3$ films with 7 nm thickness.